

# RSC Advances



This is an *Accepted Manuscript*, which has been through the Royal Society of Chemistry peer review process and has been accepted for publication.

*Accepted Manuscripts* are published online shortly after acceptance, before technical editing, formatting and proof reading. Using this free service, authors can make their results available to the community, in citable form, before we publish the edited article. This *Accepted Manuscript* will be replaced by the edited, formatted and paginated article as soon as this is available.

You can find more information about *Accepted Manuscripts* in the [Information for Authors](#).

Please note that technical editing may introduce minor changes to the text and/or graphics, which may alter content. The journal's standard [Terms & Conditions](#) and the [Ethical guidelines](#) still apply. In no event shall the Royal Society of Chemistry be held responsible for any errors or omissions in this *Accepted Manuscript* or any consequences arising from the use of any information it contains.



## The polymeric nanofilm of triazinedithiolsilane capable of resisting corrosion and serving as an activated interface on copper surface

Received 21st September 2015,  
Accepted 00th November 2015

DOI: 10.1039/x0xx00000x

www.rsc.org/

Yabin Wang,<sup>ab</sup> Zhong Liu,<sup>b</sup> Yaping Dong,<sup>b</sup> Wu Li,<sup>b</sup> Yudong Huang<sup>\*a</sup>, Yutai Qi<sup>\*a</sup>

It seems self-contradictory for a copper surface to resist corrosion and to be activated concurrently. On the one hand, the activated surface has a high affinity with water (H<sub>2</sub>O) and chloridion (Cl<sup>-</sup>) that severely accelerate the corrosion; on the other hand, only inert/unactivated/hydrophobic surfaces can exhibit outstanding corrosion resistance. This investigation concentrates on fabricating a novel multifunctional polymeric nanofilm which can resist corrosion and serve as an activated interface on copper surface simultaneously, as well as revealing the nanofilm's functional mechanism. One of the triazinedithiolsilane compound (TESPA) was self-assembled onto copper surface along with the following heating to obtain such a multifunctional interface. In order to explore the protective ability, octadecyltrichlorosilane (OTS) that can yield hazardous substance to copper was selected to be anchored, forming the bilayer of TESPA-OTS. To confirm the activating capability of the polymeric nanofilm, octyltriethoxysilane (OTES) as a friendly reagent was grafted onto the surface (TESPA-OTES). Electrochemical tests were applied to evaluate the corrosion resistance of the bilayers, contact angle (CA) was carried out to monitor the wetting property/chemical group changes, scanning electron microscope (SEM) was adopted to observe the morphologies, and energy dispersive X-ray spectroscopy (EDS) to detect the chemical states. The results from the comparison experiments show that OTS and OTES can be successfully anchored to the functionalized copper surface via SiOH groups originated from the polymeric nanofilm; the disulfide units (-SS-) and siloxane networks (SiOSi) efficiently protect the copper surface. In short, the investigation definitely proves that the polymeric nanofilm not only protects the copper, but also serves as an activated interface on copper surface. This multifunctional interface is expected to open up the possibilities for other OH-containing reagents to be anchored onto copper surface in demanding researches or industrial applications, such as catalysis, coloring and paint processes that need a protective and activated medium for higher performances.

### 1. Introduction

In the first part, we have proposed a novel design route to synthesize new kind of inhibitors that can be applied to resist corrosion for different metals<sup>1</sup>. By assembling protective triazinedithiol (TDT) and silane groups, triazinedithiolsilane compounds capable of protecting copper have been successfully prefabricated. 6-(3-triethoxysilylpropyl) amino-1, 3, 5-triazine-2, 4-dithiol monosodium salt (TESPA-TDT, abbreviated as TESPA) is just one of such triazinedithiolsilane compounds. The polymeric nanofilm prepared by heating the self-assembled monolayer (SAM) of TESPA, protects

copper from corroding with satisfactory inhibition efficiency. The preparation process of TESPA polymeric nanofilm is shown in Figure S1.

In the second part<sup>2</sup>, the chemical reactions between TESPA monomer and copper substrate, as well as the component changes during the process of preparing the polymeric nanofilm were unravelled by X-ray photoelectron spectroscopy (XPS). The results show that -SS- units and SiOSi networks act as the protective structures. Furthermore, the contact angle measurement exhibits high hydrophilic abilities of the TESPA-containing copper surfaces owing to the silanol groups atop the nanofilms. In these two studies, a bare copper and another one heated at elevated temperature under oven were used as reference samples; a TESPA treated copper surface and a TESPA treated one with heating were compared. For simplification, the abbreviations of the four surfaces are as follows: Cu-Bare, Cu-Heat, Cu-TESPA (the TESPA SAM), and Cu-TESPA-Heat (the TESPA polymeric nanofilm). It should be concretely pointed out that although an activated interface on copper surface

<sup>a</sup>School of Chemical Engineering and Technology, Harbin Institute of Technology, Harbin 150001, P. R. China. E-mail: ydhuang.hit1@aliyun.com; inqdsd@yahoo.com.cn. Tel.: +86 451 86414806; fax: +86 451 86221048.

<sup>b</sup>Qinghai Institute of Salt Lakes, Chinese Academy of Sciences, Xining, Qinghai 810008, P. R. China.

has been developed during the process, leading to hydrophilic surfaces of polar SiOH groups both in Cu-TESPA and Cu-TESPA-Heat, the protective structures of disulfide units (-SS-) and siloxane networks (SiOSi) only develop by heating the TESPA SAM.

The former investigations only emphasized the corrosion resistance and chemical mechanism. As we penetrate into the unique texture of the TESPA polymeric nanofilm, we suppose that the polymeric nanofilm can resist corrosion and serve as an activated interface on copper surface concurrently in theory. Consequently, this work will shed light on its multifunctionality. In order to evaluate the activating ability, octadecyltrichlorosilane (OTS) and octyltriethoxysilane (OTES) are chosen to react with the functionalized interface, because these two silanes can hydrolyze and produce SiOH groups which theoretically provide the active sites for the upcoming reaction with SiOH groups from the TESPA polymeric nanofilm. In the case of estimating the protective capability, the corrosion resistance of bilayers obtained from grafting OTS and OTES were compared. This design (the choice of OTS and OTES) depends on the chemical characteristics of the two reagents. OTES with octyl group belongs to a kind of alkoxy silanes and its hydrolysis by-product is alcohol, which makes OTES environmentally friendly and extensive applied as corrosion inhibitor for metals<sup>3</sup>. OTS with octadecyl group, as one of chlorosilanes, would produce hydrogen chloride (HCl) during the grafting procedure, if it can be anchored onto the SiOH-containing surfaces. It was reported that the concentration of HCl on the substrate surface was very high and the local pH could even reach 0.5 ~ 1<sup>4</sup>. These numerous HCl would cause serious corrosion on metal substrates by both H<sup>+</sup> and Cl<sup>-</sup>. In this study, we also pre-modified copper surface directly with OTS (see Figure S2 in support information). Figure S2 show the SEM images of copper surface modified directly with OTS with 5 μm and 1 μm. It is clear that lots of amorphous white particles (Figure S2b) emerge and distributed on the copper surface (Figure S2a). The copper surface is seriously destroyed compared with the bare one (Figure S2c and Figure S2d). The white particles were also

analyzed with EDS in Figure S3. Chlorine with high content exists in these particles and the surface without the white particles excludes Cl, which demonstrates that the white particles are the products of reaction between copper and OTS. As a result, few studies utilized OTS as protector for metals<sup>5-7</sup>, which makes grafting OTS on copper surface worthwhile and meaningful in this study. Besides, silanes could only be chemically anchored to hydroxyl-containing metal surfaces (-OH), such as stainless steel and aluminium. It is impossible to directly graft silanes onto copper due to the inexistence of OH groups on the surface<sup>5-7</sup>. This study somehow attempts to demonstrate a feasible route to graft this kind of compound onto the copper surface.

Assuming OTS and OTES can be successfully anchored onto the TESPA-containing interfaces (i.e., the activating ability realizes), copper surfaces with TESPA SAM and the TESPA polymeric nanofilm are designed to be treated by the above silanes, with the purpose of revealing the protective role of the disulfide units (-SS-) and siloxane networks (SiOSi). Taking OTS as an example, both the Cu-TESPA and Cu-TESPA-Heat were immersed into OTS solution, leading to Cu-TESPA-OTS and Cu-TESPA-Heat-OTS surfaces. In addition, both Cu-TESPA-OTS and Cu-TESPA-Heat-OTS surfaces were cured to explore the protective ability of newly formed siloxane networks between the silane reagents and the TESPA-containing surfaces. Thus, four surfaces obtained from OTS or OTES treatment are prepared in the experiment, exhibited in Table 1.

**Table 1** The designed comparative experiments of the TESPA-containing surfaces treated with OTS and OTES. Cu-TESPA stands for copper surface covered with TESPA SAM, and Cu-TESPA-Heat represents copper surface covered with TESPA polymeric nanofilm. For example, when the surface coated with TESPA SAM is immersed in OTS solution, it will be marked with Cu-TESPA-OTS. Upon heating, Cu-TESPA-OTS turns into Cu-TESPA-OTS-Heat, and so forth.

Experiment	Surface 1	Surface 2	Surface 3	Surface 4
OTS	Cu-TESPA	Cu-TESPA	Cu-TESPA-Heat	Cu-TESPA-Heat
	-OTS	-OTS-Heat	-OTS	-OTS-Heat
OTES	Cu-TESPA	Cu-TESPA	Cu-TESPA-Heat	Cu-TESPA-Heat
	-OTES	-OTES-Heat	-OTES	-OTES-Heat

## 2. Experimental

### 2.1. Preparing TESPA SAM and the TESPA polymeric nanofilm

The TESPA self-assembly solution consists of 3 mM TESPA monomer dissolved in ethanol/distilled water (95/5, v/v) mixed solvent, with PH of 5 by adding acetic acid examined by means of pH meter. The solution was stirred adequately and hydrolyzed for 15h at 35°C. Millipore-Q water (18.2 MΩ cm) was used in all solutions. Unless noted otherwise, all reagents used were of analytical grade. The pure copper plates, cut into the dimensions of 20 mm by 20 mm and 1 mm thick for electrochemical examinations, were abraded with emery paper of 1000 grit and 800 grit, and followed by fine polishing with alumina paste of 0.35 μm, 0.2 μm, 0.1 μm particle size to achieve a mirror finish. The samples then

degreased with acetone and alcohol in an ultrasonic bath for 15 min, and finally rinsed with copious Millipore-Q water. After cleaning, the copper specimens were immediately immersed in TESPA solution for 15 min, thoroughly rinsed with ethanol and pure water, and finally dried by cold air from a hair dryer (TESPA SAM), aged at 100°C for 15 min in an air oven (the TESPA polymeric nanofilm). Herein, a bare copper and another one heated at 100°C for 15 min were used as reference samples.

The copper samples were then immersed (dip coating method) into the OTES solution or the OTS solution for 15min<sup>8</sup>, then rinsed sequentially with ethanol and pure water to remove the unbound SAM, and finally dried by cold air. The OTS solution consists of 3 mM OTS dissolved in anhydrous toluene and was stirred for 2 hours. OTES (3 mM) was dissolved in ethanol (95%) and hydrolyzed for 15 h at a pH of ca. 4<sup>9</sup>.

### 2.2. Electrochemical measurements

Electrochemical measurements were conducted on an Autolab workstation (Netherlands) in a standard three-electrode system at  $25 \pm 1^\circ\text{C}$ . A solution of 3.5 wt% NaCl used as electrolyte was not deoxygenated and open to the air during each test process. The obtained specimens were successively adopted as the working electrode with an exposed area of  $0.785\text{ cm}^2$  (a circle with 1cm diameter) to the NaCl solution. A saturated calomel electrode (SCE) with a salt bridge in a Luggin capillary serves as the reference electrode and a platinum panel ( $2\text{ cm}^2$ ) as the counter electrode. All potential values were referred to  $E_{\text{SCE}}$ . Cyclic voltammetry (CV) was performed through scanning the potential from  $-0.7\text{ V}$  to  $0.6\text{ V}$  with a sweep rate  $10\text{ mV/s}$ . Electrochemical Impedance Spectroscopy (EIS) was carried out in the frequency range from  $100\text{ kHz}$  to  $10\text{ mHz}$  with 100 points at a  $10\text{ mV}$  amplitude of the excitation signal under the open circuit potential ( $E_{\text{ocp}}$ ). All EIS data were collected after immersing the working electrodes in the electrolyte for 50 min to reach a stable situation<sup>1</sup>. The potentiodynamic polarization curves (Tafel) were recorded from  $E_{\text{ocp}} - 350\text{ mV}$  to  $E_{\text{ocp}} + 350\text{ mV}$  at a scan rate of  $1\text{ mV/s}$ . Before the data were recorded, the tested coupons were also immersed in the electrolyte for 50 min in an attempt to achieve a steady state.

### 2.3. The equivalent circuits and contact angle

By comparing experimental data with the simulated, the configurations of equivalent circuits (EC) concerning the TESPA-containing surfaces were tested using ZSimpWin software. The quality of EC was first judged by chi-square ( $\chi^2$ ) value, and second by error distribution. Contact angle measurements were performed on a contact angle analyzer, XG-CAMB manufactured by Xuanyichuangxi Industrial Equipment Co., Ltd. (China, Shanghai). The data were collected at five different points on each sample surface resulting in an average value.

### 2.4. Scanning electron microscopy (SEM) and energy-dispersive spectroscopy (EDS)

SEM-EDS study was performed at JSM-5610LV/INCA (JEOL Ltd., Japan), using a high-resolution environmental scanning electron microscope equipped with an energy-dispersive X-ray spectrometer (EDAX, Japan). Energy dispersive spectroscopy of the each surface was carried out in random areas for five times to identify the existed elements and their contents, which can further confirm the uniform coverage of the nanofilms.

## 3. Results and discussion

### 3.1. Grafting OTS onto TESPA-containing surfaces

#### 3.1.1. Grafting OTS onto TESPA SAM surface

In order to elucidate the protective capability of the nanofilms obtained by treating the TESPA SAM with OTS, CV, Tafel and EIS tests were conducted. On the whole, the curves of the OTS modified Cu-TESPA (TESPA SAM) without/with heating from the three measurements can be easily differentiated from the Cu-TESPA, indicating that OTS can react with the TESPA SAM. That is, OTS can be successfully anchored onto the TESPA SAM interface via SiOH groups from both reactants. Fig. S4 shows the current of the four samples as a function of potential in CV test. It can be seen that a big oxidation peak, including the oxidation of Cu(I) to soluble Cu(II) species, copper oxide or hydroxychloride<sup>10</sup>, occurs in the

positive scan for bare copper. A large reduction peak observed in the reverse sweep corresponds to the reduction of the soluble copper complex. Cu-TESPA sample possesses a quasi shape of oxidation and reduction peaks. However, the intensive decrease of the peak area and peak height indicates that the TESPA SAM efficiently protects copper. When OTS is grafted onto the surface, the peak area and peak height in CV curve of the Cu-TESPA-OTS slight boost, but are still smaller/lower than that of the Cu-Bare. This phenomenon demonstrates that the TESPA SAM is damaged and the protective ability becomes inferior, or the copper is corroded during the process of grafting OTS onto Cu-TESPA. Considering that OTS can undergo reaction with silanol groups from the TESPA SAM, it is most likely that the yielded harmful product (HCl) corrodes the copper and impairs protective capability. Upon heating the Cu-TESPA-OTS, the plot turns to be the same as that of the Cu-TESPA, suggesting the limited fortification of the corrosion resistance. Hence, it can be concluded that the disulfide units (-SS-) resist corrosion which develop through thermal polymerization<sup>1</sup>, but the protective functionality of the siloxane networks (SiOSi) cannot be clarified in this procedure.

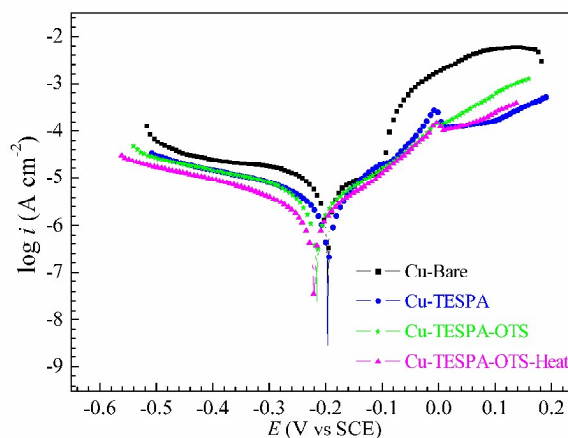


**Fig. 1** Polarization plots of the bare copper (Cu-Bare), copper treated with TESPA (Cu-TESPA), TESPA-coated copper modified with OTS (Cu-TESPA-OTS), and TESPA-coated copper modified with OTS plus following heating (Cu-TESPA-OTS-Heat) in 3.5 wt% NaCl solution. Cu-TESPA stands for copper surface covered with TESPA SAM.

Fig. 1 presents the changes in Tafel plots of the four samples. The anodic polarization curve for bare copper can be split into three main regions, an apparent Tafel region close to the corrosion potential (the formation of CuCl ad-layer), a limiting-current region with an anodic current peak centred around  $+0.095\text{ V}$  (the dissolution of CuCl film), and a mixed-kinetics region above the limiting-current potential (the formation of divalent copper species)<sup>11</sup>. Cu-TESPA leads to remarkable decline of anodic and cathodic currents, implying that the TESPA SAM significantly inhibits the anodic dissolution and protect the copper. The Tafel plot of Cu-TESPA-OTS is nearly the same as that of the Cu-TESPA. The heated OTS-covered TESPA SAM provides better corrosion protection than OTS-modified TESPA SAM without heating. In general, Tafel result is in a good agreement with results from the CV and the interpretations presented in the earlier section. It should be also mentioned that OTS possesses a long alkyl chain composed of

eighteen carbons and the chlorosilane. The reaction between the chlorosilane moiety and silanol groups from the TESPA SAM gives rise to the outer arrangement of the long chain, i.e., the long alkyl chain atop the nanofilms. The hydrophobic properties of TESPA-OTS surfaces act as another contribution for OTS-anchored bilayers to resist corrosion. This aspect will be discussed in contact angle test.

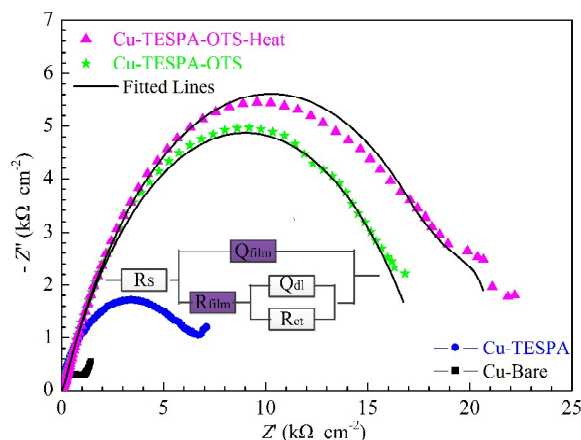


**Fig. 2** The Nyquist impedance diagrams of the bare copper (Cu-Bare), copper treated with TESPA (Cu-TESPA), TESPA-coated copper modified with OTS (Cu-TESPA-OTS), and TESPA-coated copper modified with OTS plus following heating (Cu-TESPA-OTS-Heat) in 3.5 wt% NaCl solution. The inset is the equivalent circuit (EC) of the OTS-modified TESPA-containing copper surfaces. Cu-TESPA stands for copper surface covered with TESPA SAM.

EIS was also performed to understand the electrochemical behaviour of the four samples in Fig. 2. The Nyquist impedance diagram of the bare copper consists of a depressed semicircle at the high frequency and a straight line at low frequency. The semicircle, caused by the charge transfer process, is related to the time constant of the charge-transfer resistance ( $R_{ct}$ ) and the double-layer capacitance ( $C_{dl}$ ) at the interface of copper/NaCl solution<sup>1,12</sup>. When the semicircle is depressed, it can be accredited to the frequency dispersion that exerts by the inhomogeneity and roughness of substrate surface<sup>13</sup>. The straight line typically known as Warburg impedance can be ascribed to the anodic diffusion process of copper chloride compounds from the electrode surface to the bulk solution<sup>14</sup>, the presence of which indicates that diffusion dominates rather than charge transfer process under this circumstance. For Cu-TESPA, the Warburg impedance still exists at low frequencies, but the capacitive loop becomes large, indicating that the TESPA SAM is densely packed to hinder the diffusion. For both OTS-anchored copper surfaces without/with heating, the Warburg impedances disappear at low frequencies. Observation of only large capacitive loops shows that the processes of the two samples are controlled by charge transfer instead of diffusion process, which is entirely different from the reference and Cu-TESPA samples, revealing that the bilayers are more densely packed to hinder the diffusion. The improvement of the diameter for capacitive loop in Cu-TESPA-OTS-Heat than Cu-TESPA-OTS, displays a better corrosion inhibition; it suggests the formation of the disulfide units (-SS-) as

TESPA SAM on copper surface is heated. The regularity of EIS consistent with Tafel result further substantiates the best protective performance of the heated Cu-TESPA-OTS surface.

In order to decipher the difference of the bilayers (TESPA-OTS), the equivalent circuits (EC) of the OTS-treated Cu-TESPA without/with heating are also carried out, and given in Figure 2. The quality of EC was first judged by chi-square ( $\chi^2$ ) value, and second by error distribution. All the references' EC excluded here can be found in Part one<sup>1</sup>. An excellent agreement can be observed between the experimental data (points) and the fitted curve (solid line). The  $\chi$  of the OTS-treated Cu-TESPA without/with heating calculated by ZWinWin software is below  $10^{-3}$ . Combined with the observation of only large capacitive loops (the charge transfer dominates), it is reasonable to use the circuit  $R(Q(RRQ))$  for the two nanofilms. The calculated values of each element in the equivalent circuits are listed in Table 2, where  $R_s$ ,  $R_{film}$  and  $R_{ct}$  is the solution resistance, resistance of coating and charge transfer resistance;  $Q_{film}$  and  $Q_{dl}$  stand for capacitance of coating and capacitance of copper/solution interface, respectively.

### 3.1.2. Grafting OTS onto the TESPA polymeric surface

According to Figure S1, it is easy to find out that polymeric TESPA nanofilm possesses an inherent advantage compared to TESPA SAM. The preferentially formed texture composed of disulfide units and SiOSi networks protect the surface and blocks other chemical substances to some extent<sup>1</sup>. However, comparatively speaking, the disadvantage embodies in the decrease number of the SiOH groups that provide active sites for the subsequent chemical reactions. Whether the residual SiOH groups can graft enough OTS to form the super protective coating is still worth probing into.

In order to clarify these issues about the protective capability of the TESPA polymeric nanofilm, CV, Tafel and EIS tests of the OTS-treated TESPA polymeric nanofilm (Cu-TESPA-Heat) were also carried out. Herein, Cu-TESPA-Heat is added into all the curves as a new reference. As a whole, the curves of the OTS modified Cu-TESPA-Heat with/without heating from the three measurements can be easily differentiated from the Cu-TESPA-Heat, revealing that OTS can react with the TESPA polymeric nanofilm, although the number of SiOH groups is fewer than that of the TESPA SAM. OTS can be successfully anchored onto the TESPA polymeric nanofilm through the residual SiOH groups.

Fig. S5 shows the current of the five samples as a function of potential in CV test. It can be seen that the TESPA polymeric nanofilm further protect copper surface, consistent with the result in Part one. When this surface is modified with OTS, the peak area and peak height in CV curve of the Cu-TESPA-Heat-OTS slight boost, but are still smaller/lower than that of the Cu-Bare. Upon heating the surface, the peak area and peak height turn out to be the smallest, suggesting a significant enhancement of corrosion resistance. Compared with OTS-modified TESPA SAM without/with heating in Figure S4, the OTS-treated TESPA polymeric nanofilms present a stronger resistant ability. It can be concluded that the formed -SS- units and SiOSi networks preferentially protect the surface.

The changes in Tafel plots of the five samples were compared in Fig. 3. Cu-TESPA-Heat leads to remarkable decline of anodic and cathodic currents, implying that the polymeric nanofilm significantly inhibits the anodic dissolution and protects the copper. After coating

OTS on the TESPA polymeric nanofilm, the resultant bilayers further resist corrosion. However, the curves of the OTS-anchored Cu-TESPA-Heat without/with heating are indistinct, compared with the difference of the OTS-anchored Cu-TESPA (see Fig. 1). This subtle imparity stems from the grafting amount of OTS; the TESPA polymeric nanofilm affords less SiOH groups for the subsequent reactive sites.

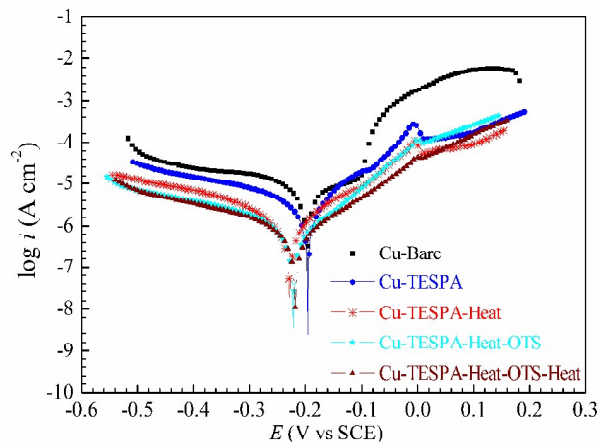


**Fig. 3** Polarization plots of the bare copper (Cu-Bare), copper treated with TESPA (Cu-TESPA), copper treated with TESPA plus the following heating (Cu-TESPA-Heat), TESPA-coated copper modified with OTS (Cu-TESPA-Heat-OTS), and TESPA-coated copper modified with OTS plus the following heating (Cu-TESPA-Heat-OTS-Heat) in 3.5 wt% NaCl solution. Cu-TESPA stands for copper surface covered with TESPA SAM, and Cu-TESPA-Heat represents copper surface covered with TESPA polymeric nanofilm.

EIS was also performed to understand the electrochemical behaviour of the five samples in Fig. 4. The enhancement of the capacitive loops from the OTS-treated Cu-TESPA-Heat without heating to the heated one confirms the increased protective ability. For the TESPA polymeric nanofilm and the OTS-treated Cu-TESPA-Heat surfaces, the appearance of only capacitive loops

implies the charge transfer dominates. Therefore, the equivalent circuits of the OTS-treated Cu-TESPA-Heat without/with heating are similar to that of the OTS-treated Cu-TESPA, and can be expressed with  $R(Q(R(RQ)))$  as well. The calculated values of each element in the equivalent circuits are also listed in Table 2.

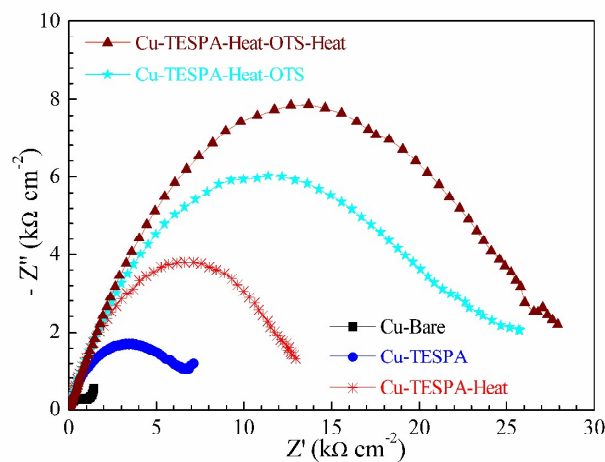


**Fig. 4** The Nyquist impedance diagrams of the bare copper (Cu-Bare), copper treated with TESPA (Cu-TESPA), copper treated with TESPA plus the following heating (Cu-TESPA-Heat), TESPA-coated copper modified with OTS (Cu-TESPA-Heat-OTS), and TESPA-coated copper modified with OTS plus the following heating (Cu-TESPA-Heat-OTS-Heat) in 3.5 wt% NaCl solution. Cu-TESPA stands for copper surface covered with TESPA SAM, and Cu-TESPA-Heat represents copper surface covered with TESPA polymeric nanofilm.

### 3.1.3. The difference of the bilayers

**Table 2** Values of the elements in equivalent circuit to fit EIS for the OTS-modified TESPA SAM and polymeric nanofilm. Cu-TESPA stands for copper surface covered with TESPA SAM, and Cu-TESPA-Heat represents copper surface covered with TESPA polymeric nanofilm.

Sample	Cu-TESPA -OTS	Cu-TESPA -OTS-Heat	Cu-TESPA-Heat -OTS	Cu-TESPA-Heat -OTS-Heat
Chi-square ( $\chi^2$ )	$3.72 \times 10^{-3}$	$5.36 \times 10^{-3}$	$4.66 \times 10^{-3}$	$5.19 \times 10^{-3}$
Circuit	$R(Q(R(RQ)))$	$R(Q(R(RQ)))$	$R(Q(R(RQ)))$	$R(Q(R(RQ)))$
$R_s$ ( $\Omega \text{ cm}^2$ )	16.27	14.54	8.63	8.16
$Q_{\text{film}}$ ( $\text{S s}^n \text{ cm}^{-2}$ )	$3.05 \times 10^{-5}$	$2.05 \times 10^{-5}$	$1.48 \times 10^{-5}$	$1.22 \times 10^{-5}$
$n_{\text{film}}$	0.80	0.61	0.61	0.59
$R_{\text{film}}$ ( $\Omega \text{ cm}^2$ )	295	524	1110	1661
$Q_{\text{dl}}$ ( $\text{S s}^n \text{ cm}^{-2}$ )	$1.02 \times 10^{-5}$	$6.39 \times 10^{-6}$	$9.12 \times 10^{-7}$	$6.05 \times 10^{-8}$
$n_{\text{dl}}$	0.80	0.74	0.83	0.88
$R_{\text{ct}}$ ( $\Omega \text{ cm}^2$ )	$1.79 \times 10^4$	$1.97 \times 10^4$	$2.34 \times 10^4$	$2.94 \times 10^4$

From the data in Table 2, it is clear that the resistance of coating ( $R_{\text{film}}$ ) and charge transfer resistance ( $R_{\text{ct}}$ ) gradually increase, indicating the protective abilities become stronger. Conclusions can be drawn that: (1) Compared with the TESPA SAM, the TESPA polymeric nanofilm hinders HCl more efficiently throughout the interface damaging the substrate, due to the preferentially formed disulfide units (-SS-) and siloxane networks (SiOSi). (2) The heated

surface of the OTS-anchored TESPA polymeric nanofilm holds a higher corrosion resistance than OTS-anchored TESPA polymeric nanofilm without heating. The result reveals that the hydrolyzed OTS adsorb on TESPA polymeric nanofilm via SiOH from both entities, and another new protective structure of siloxane networks (SiOSi) develops when the OTS-anchored Cu-TESPA-Heat is curing. For a given coating, the changes in  $Q_{\text{film}}$  are often taken as a measure of water uptake in the coating<sup>15</sup>.  $Q_{\text{film}}$  decreases from the

unheated surfaces to the heated surfaces (from surface 1 to surface 4), demonstrating that the adsorption of water onto the latter three nanofilms becomes harder. The result attributes to the decline of hydrophilic SiOH groups that condenses among themselves via losing water at the elevated temperature, the formation of SiOSi network which provides the three dimensional cross-linking structure as a barrier to block the penetration of water molecules, and the long hydrophobic alkyl chain atop the bilayers. Meantime, when copper surface is treated with the order from surface 1 to surface 4,  $Q_{dl}$  values decrease a order of magnitude successively, which can be ascribed to a decrease of dielectric constant due to the adsorption of OTS and the structural change (the formation of SiOSi and SS) of nanofilm<sup>16</sup>.

Fig. 5 shows the phase angle plot for the OTS modified TESP SAM and the TESP polymeric nanofilms without/with heating. As observed earlier, one time constant appears in the phase angle plot for the bare copper. TESP SAM and the polymeric nanofilm possess two time constants; the OTS-treated TESP SAM and the polymeric nanofilm have two time constants as well. However, in comparison, the additional time constants of the OTS-treated TESP SAM and the polymeric nanofilm are more evident than that of the only TESP-containing nanofilms (see Figure 7 in Part one<sup>1</sup>). Hereon, when the TESP polymeric nanofilm are treated with OTS, the angles at high frequencies increase compared with the OTS-modified TESP SAM that have abrupt and distinct ones, giving rise to relatively flattening curves. Generally, the appearance of an additional time constant implies the formation of some new, highly water-resistant structure at the interface of the substrate and nanofilm. The plausible explanation is that the number of SiOH groups determines the behaviour of the phase angle plots; SiOH groups reduce by condensing with one another as TESP SAM is cured.

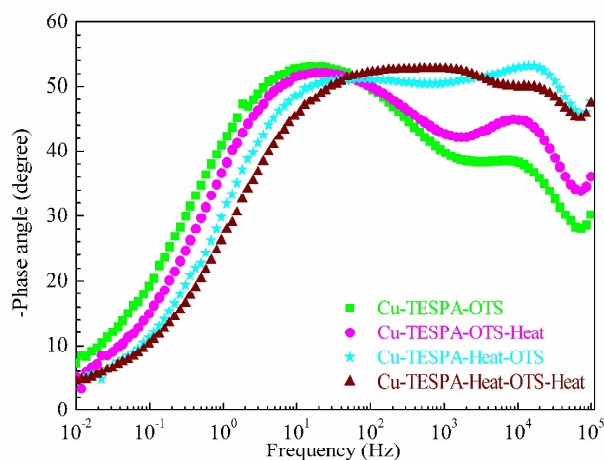


**Fig. 5** The phase angle plots of the OTS-modified TESP SAM without heating (Cu-TESPA-OTS), OTS-modified TESP SAM plus heating (Cu-TESPA-OTS-Heat), OTS-modified TESP polymeric nanofilm without heating (Cu-TESPA-Heat-OTS), and OTS-modified TESP polymeric nanofilm plus heating (Cu-TESPA-Heat-OTS-Heat) in 3.5 wt% NaCl solution. Cu-TESPA stands for copper surface covered with TESP SAM, and Cu-TESPA-Heat represents copper surface covered with TESP polymeric nanofilm.

### 3.1.4. The contact angles

The changes of functional groups on copper surfaces, or the functional groups atop the nanofilms, were monitored with contact angles shown in Fig. 6. When bare copper with a contact angle of 63.1° is heated under atmospheric environment in an oven, a copper oxide layer develops with an increased contact angle of 84.6°. As for Cu-TESPA surface, the value declines to 44.7° exhibiting high hydrophilic ability because numerous SiOH groups are outer at the top of the SAM. The contact angle of the Cu-TESPA-Heat is 69.3° and becomes less hydrophilic, implying that polar silanol groups decline and cross-link to SiOSi network atop the nanofilm as a result of the condensation reaction at high temperature. These phenomena manifest the structural arrangements of the nanofilm on both Cu-TESPA and Cu-TESPA-Heat surfaces, namely, the silane part in TESP is located on top of the TESP SAM or the TESP polymeric nanofilm, and trianedithiol groups at the bottom (as the interfacial layer between copper and the nanofilms).

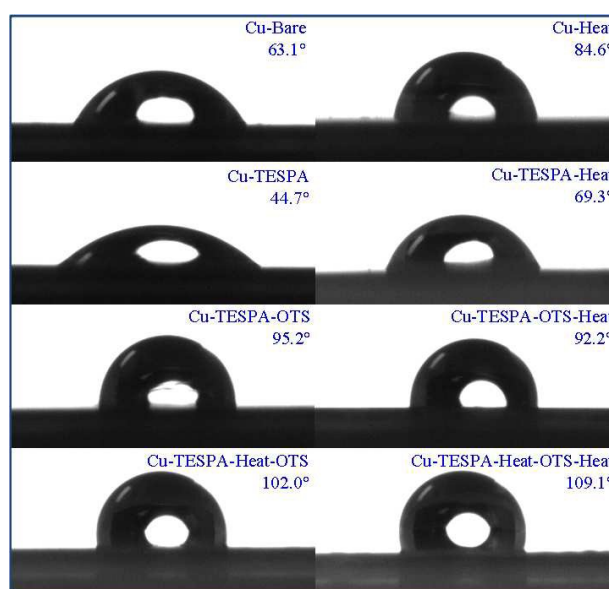


**Fig. 6** Contact angles of the references (the top four surfaces), the OTS-modified TESP SAM and the polymeric nanofilms. Cu-TESPA stands for copper surface covered with TESP SAM, and Cu-TESPA-Heat represents copper surface covered with TESP polymeric nanofilm.

When OTS was coated on TESP-containing surfaces, the contact angles greatly improved and the surfaces turn to be hydrophobic ( $> 90^\circ$ ), indicative of successful attachment of OTS to the SiOH groups from the TESP nanofilms. The contact angles from the OTS-anchored TESP polymeric nanofilms outweigh the ones from the OTS-anchored TESP SAM, coincident with the change rule that the contact angle of TESP SAM becomes larger when heated to yield the TESP polymeric nanofilm. As is known, the wettability of solid surfaces is governed by their surface geometrical structures and surface free energy<sup>17</sup>. When bare copper is only heated, the contact angle changes from 63.1° to 84.6°, indicating the surface structure particularly varies, supporting by the SEM image in Part two. As the TESP SAM is cured, the contact angle transforms from 44.7° to 69.3°, which suggests that the SiOH groups condense with each other and the number of them dramatically decrease by XPS result earlier. Thus, these two aspects

lead to the relatively large difference between the OTS-modified TESPAM SAM and the polymeric nanofilm. Since the hydrophobic property is closely related to the micro- and nano- structure, detailed information about the structural change of OTS-coating surface will be explored as part of our upcoming investigations.

### 3.1.5. Scanning electron microscopy (SEM)

In order to entirely understand the surface morphology and microstructure of the investigated surfaces, scanning electron microscopy was performed with different scanning scales. Fig. S6 and 7 illustrate the SEM micrographs of 5  $\mu\text{m}$  and 1  $\mu\text{m}$  for the bare copper, the heated copper, the copper treated with TESPAM, TESPAM-treated copper along with following heating, OTS-modified TESPAM SAM without/with heating, and OTS-modified TESPAM polymeric nanofilm without/with heating, respectively. Fig. S6a and 7a show the initial surface state of the polished bare substrate. The surface is considerably rough, some fine streaks resulting from the polishing process are visible, and plenty of white spots are obvious. The white spots are solely “carbon contaminations” from fabricating procedure (This was confirmed by utilizing EDS on the white spots in Figure S7 from the supporting information). As the bare substrate is heated, lots of the white spots disappear because the carbon contaminations are oxidized under the atmosphere at high temperature. The streaks become clearer (Fig. S6b) and seem to be filled (Fig. 7b) owing to the coverage of copper oxide in these areas. The TESPAM-treated copper surface turns out to be smoother than that of the former surfaces (see Fig. S6c), and the enlarged view with 1  $\mu\text{m}$  from Fig. 7c displays that the surface is uniformly covered with TESPAM self-assemble monolayer. The disappearance of the white spots can be ascribed to the coverage of TESPAM monomers on bare copper. No apparent changes can be observed when the TESPAM-treated copper surface is heated, i.e., the surface is still smoother and uniformly covered, as shown in Fig. S6d and Fig. 7d. The OTS-treated TESPAM-

containing surfaces show great difference, compared with the untreated ones. Quite a number of white particles emerge on the surfaces of the OTS-modified TESPAM SAM without/with heating (Fig. S6e and S6f). In the 1  $\mu\text{m}$  micrographs, the sizes of these white particles are larger than that of the bare one's. The white particles are the products of reaction between TESPAM and OTS. They have high content of chlorine, while the flat sites are mainly TESPAM film (see Figure S8 in supporting information).

In order to thoroughly understand the origin of the white particles, EDS element mapping was carried out for the TESPAM and OTS-modified copper surface (see Figure S9 in supporting information). It clearly reveals that C and Cl elements are highly contained in the particles. Copper surface without particles is uniformly covered by bilayer of TESPAM and OTS. These observations manifest not only that the white particles are the products of reaction between TESPAM and OTS, but also TESPAM SAM primarily reacts with OTS and protect the copper substrate. Noticeably, the morphologies of the white spots (Fig. S7), the white particles from copper surface directly modified with OTS (Fig. S3), and the white particles from TESPAM-covered surface modified with OTS (Fig. S8) are variant, revealing that they are different compounds. Even though heating the OTS-modified TESPAM SAM, the formed bilayer cannot resist corrosion well, because the surface has been damaged already. White particles are still full of the surface of the OTS-modified TESPAM polymeric nanofilm without heating (Fig. S6g), however, the number greatly declines and the shape is close to the bare (Fig. 7g). It can be concluded that the TESPAM polymeric nanofilm resist corrosion to some extent; the pre-yielded disulfide units (-SS-) and siloxane networks (SiOSi) act as the protective structure. Upon curing, the white spots in Fig. S6h are difficult to observe, indicating the heated OTS-modified TESPAM polymeric nanofilm extremely hinders the corrosion (Fig. 7h).

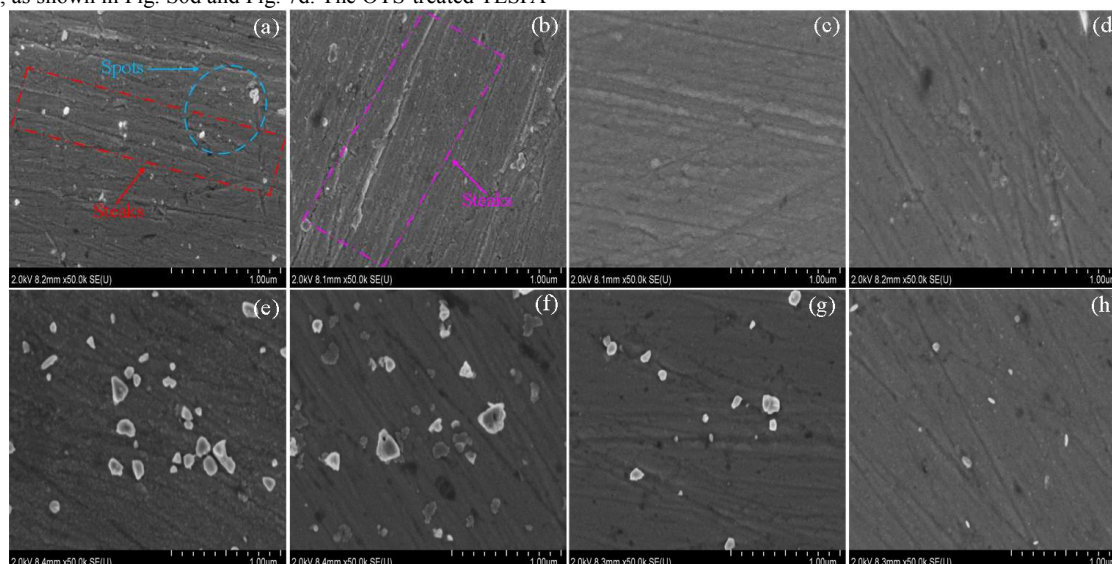


**Fig. 7** SEM micrographs with 1  $\mu\text{m}$  of the (a) bare copper, (b) heated copper, (c) copper treated with TESPAM, (d) copper treated with TESPAM plus following heating, (e) OTS-modified TESPAM SAM without

heating, (f) OTS-modified TESPAM SAM plus heating, (g) OTS-modified TESPAM polymeric nanofilm without heating, and (h) OTS-modified TESPAM polymeric nanofilm plus heating.

## ARTICLE

## RSC Advances

As we know, the difference between the OTS-modified TESPA polymeric nanofilm without heating and the heated one is the new formation of SiOSi (other aspects are same, such as the number of the SiOH groups, the octyl chain, etc.) This part originates from the OTS and the TESPA polymeric nanofilm (another SiOSi part comes from TESPA itself when it is cured). Although the number of the SiOH groups from the TESPA polymeric nanofilm decreases compared with that of the TESPA SAM, these active groups play a significant role in grafting new agents and developing siloxane networks (SiOSi) to protect copper. The SEM images of the referential and the studied surfaces offer direct evidence of visual observation that the TESPA polymeric nanofilm not only prevents copper from corroding to some degree, but also serves as an activated interface on copper surface.

### 3.1.6. Energy dispersive X-ray spectroscopy (EDS)

We carried out the energy dispersive spectroscopy of each surface in random areas for five times. The results are identical, indicating that the bilayers are uniformly distributed on copper surface. Fig. 8 is just one representative of the each examination. The existing elements, their contents, and the coefficients ( $\sigma$ ) are also listed as the inset tables. The TESPA-treated surfaces without/with heating detect new elements of S, N and Si with minor amount (Fig. 8a to Fig. 8d), revealing the formation of TESPA nanofilms on copper surfaces. Besides, chlorine (Cl) can also be observed on all the TESPA-containing surfaces from Fig. 8a to Fig. 8d. Even we thoroughly rinsed the substrates with ethanol and pure water sequentially, Cl remains existed on TESPA-containing surfaces, suggesting that the bilayer is uniformly distributed on copper surface, and only part of chlorine from OTS reacts with the TESPA SAM or polymeric nanofilm. This can also be identified by the element mapping in Figure S9.

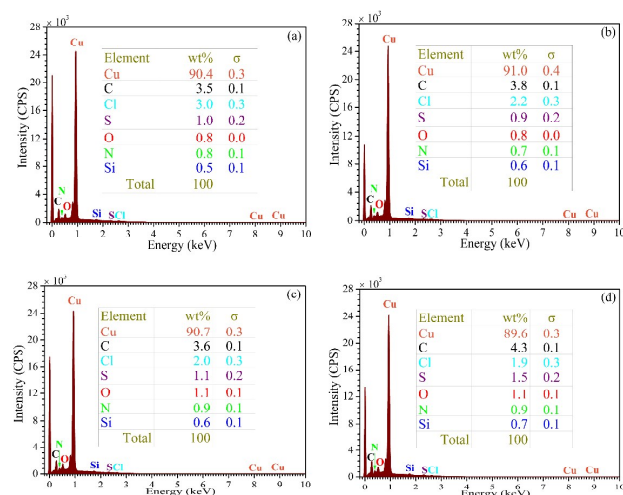


**Fig. 8** EDS spectra of the (a) OTS-modified TESPA SAM without heating, (b) OTS-modified TESPA SAM plus heating, (c) OTS-modified TESPA polymeric nanofilm without heating, and (d) OTS-modified TESPA polymeric nanofilm plus heating.

### 3.2. Grafting OTES onto TESPA-containing surfaces

In order to elucidate the activating capability of TESPA SAM and

the TESPA polymeric nanofilm, OTES as a harmless agent for copper surface was selected to be coated on these interfaces. Tafel and EIS tests were conducted; the curves of the OTES modified Cu-TESPA and Cu-TESPA-Heat without/with heating can be easily differentiated, indicating that OTES can react with the TESPA-containing surfaces. That is, OTES can be successfully anchored onto these interfaces via SiOH groups from both reactants.

#### 3.2.1. The potentiodynamic polarization curves of the OTES-modified surfaces

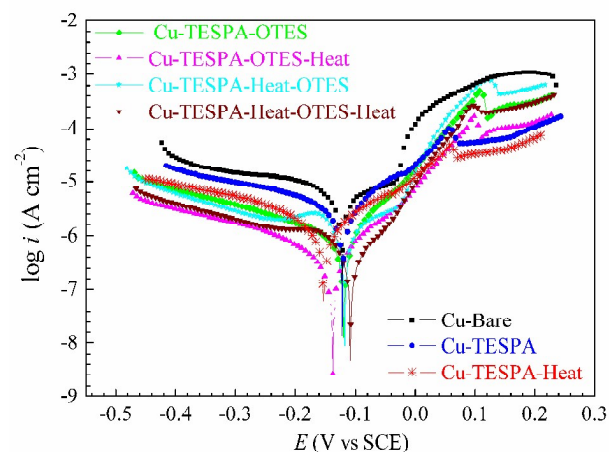


**Fig. 9** Polarization plots of the bare copper (Cu-Bare), copper treated with TESPA (Cu-TESPA), copper treated with TESPA plus the following heating (Cu-TESPA-Heat), TESPA SAM modified with OTES (Cu-TESPA-OTES), TESPA SAM modified with OTES plus heating (Cu-TESPA-OTES-Heat), the TESPA polymeric nanofilm modified with OTES (Cu-TESPA-Heat-OTES), and the TESPA polymeric nanofilm modified with OTES plus the following heating (Cu-TESPA-Heat-OTES-Heat) in 3.5 wt% NaCl solution. Cu-TESPA stands for copper surface covered with TESPA SAM, and Cu-TESPA-Heat represents copper surface covered with TESPA polymeric nanofilm.

Fig. 9 presents the changes in Tafel plots of the four samples. The curves from the OTES-modified surfaces, including both TESPA SAM and the TESPA polymeric nanofilm without/with heating, remarkably decline than that of the OTS-modified surfaces in Figure 1 and 3. In detail, the plots of the OTES-modified TESPA SAM are underneath Cu-TESPA-Heat, while the plots of the OTS-modified TESPA SAM close to Cu-TESPA (Fig. 1). The result demonstrates that the OTES-anchored TESPA SAM greatly protects the copper surface; the by-product (alcohol) originated from Cu-TESPA-OTES and the heated one does not destroy the copper substrate. The plots of the OTES-modified TESPA polymeric nanofilm and the OTS-modified ones (Fig. 3), both below the Cu-TESPA-Heat which means they protect the copper efficiently, cannot be distinguished by visual observation. However, a significant phenomenon can be seen in Fig. 9 that the OTES-modified TESPA polymeric nanofilms with heating fall in between the OTES-anchored TESPA SAM and the heated Cu-TESPA-OTES, which means that the OTES-anchored TESPA SAM plus heating owns a better corrosion resistance than that of the OTES-anchored TESPA polymeric nanofilm. It can be explained as follows: the number of the SiOH groups on the TESPA polymeric nanofilm, which provide active sites for the chemical

reactions, decrease compared with the TESPA SAM. The resultant bilayer from the polymeric nanfilm is not that densely packed compared with the one obtained from the TESPA SAM.

### 3.2.2. Electrochemical impedance spectroscopy

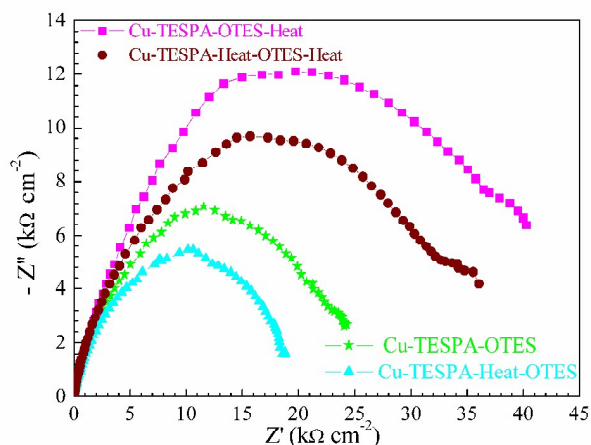


**Fig. 10** The Nyquist impedance diagrams of the TESPA SAM modified with OTES (Cu-TESPA-OTES), TESPA SAM modified with OTES plus heating (Cu-TESPA-OTES-Heat), the TESPA polymeric nanofilm modified with OTES (Cu-TESPA-Heat-OTES), and the TESPA polymeric nanofilm modified with OTES plus the following heating (Cu-TESPA-Heat-OTES-Heat) in 3.5 wt% NaCl solution. Cu-TESPA stands for copper surface covered with TESPA SAM, and Cu-TESPA-Heat represents copper surface covered with TESPA polymeric nanofilm.

EIS was performed to further comprehend the resistance structure and the protective abilities of the samples prepared by using OTES (Fig. 10). It is apparent that the capacitive loop of the

Sample	Cu-TESPA -OTES	Cu-TESPA -OTES-Heat	Cu-TESPA-Heat -OTES	Cu-TESPA-Heat -OTES-Heat
Chi-square ( $\chi^2$ )	$3.72 \times 10^{-3}$	$5.90 \times 10^{-3}$	$4.67 \times 10^{-3}$	$5.19 \times 10^{-3}$
Circuit	$R(Q(R(RQ)))$	$R(Q(R(RQ)))$	$R(Q(R(RQ)))$	$R(Q(R(RQ)))$
$R_s$ ( $\Omega \text{ cm}^2$ )	25.46	13.03	23.54	25.26
$Q_{\text{film}}$ ( $\text{Ss}^n \text{ cm}^{-2}$ )	$1.11 \times 10^{-6}$	$9.96 \times 10^{-6}$	$3.11 \times 10^{-6}$	$9.49 \times 10^{-6}$
$n_{\text{film}}$	0.81	0.57	0.81	0.58
$R_{\text{film}}$ ( $\Omega \text{ cm}^2$ )	2756	4809	2580	3716
$Q_{\text{dl}}$ ( $\text{Ss}^n \text{ cm}^{-2}$ )	$3.48 \times 10^{-5}$	$1.17 \times 10^{-5}$	$1.33 \times 10^{-6}$	$3.30 \times 10^{-7}$
$n_{\text{dl}}$	0.99	0.89	0.80	0.95
$R_{\text{ct}}$ ( $\Omega \text{ cm}^2$ )	$2.58 \times 10^4$	$4.52 \times 10^4$	$1.76 \times 10^4$	$3.68 \times 10^4$

Comparing the values of  $R_{\text{film}}$  and  $R_{\text{ct}}$  in Table 2 and 3, it is obvious that the surfaces from the heated OTES-modified TESPA SAM and the TESPA polymeric nanofilm resist corrosion more effectively than any one of the OTS-modified surfaces. OTS has a longer alkyl chain than that of the OTES, if HCl does not develop during the process of fabricating the bilayer and damage the TESPA nanofilms, it is certain that the protective ability of the bilayer with octadecyl is more powerful than that of the one with octyl, such as the second layer composed of friendly trimethoxyoctadecylsilane or triethoxyoctadecylsilane. From another point of view, the design of choosing OTS and OTES as the monomers for the grafting layers is practical and effectual. Furthermore, the  $Q_{\text{dl}}$  values from OTES-

OTES-treated TESPA SAM without heating is larger than that of the OTES-treated TESPA polymeric nanofilm without heating, as well as the capacitive loop of the OTES-treated TESPA SAM with heating outweigh the one stemmed from the OTES-treated TESPA polymeric nanofilm plus heating. In conclusion, the bilayers obtained from the Cu-TESPA protect copper more efficiently than the ones from Cu-TESPA-Heat, which is in good agreement with the interpretations from Tafel outcomes.

In order to explore the properties of the bilayers, the configurations of equivalent circuits were also carried out. On the basis of the equivalent circuits from the OTS-anchored TESPA SAM and its polymeric nanofilms, it is reasonable to use the circuit  $R(Q(R(RQ)))$  for OTES-anchored ones where the charge transfer dominates. The electrochemical parameters were listed in Table 3. As far as the OTES-coated surfaces concerned,  $Q_{\text{film}}$  irregularly changes without the rule of the OTS-coated surfaces'. To a large extent, the inconsistency is attributed to the length of the alkyl chain (octyl vs. octadecyl).  $Q_{\text{dl}}$  gradually decreases owing to the decrease of dielectric constant caused by the adsorption of OTES and the structural change (the formation of SiOSi and SS) of nanofilms, as OTS-modified surfaces exhibits.

**Table 3** Values of the elements in equivalent circuit to fit EIS for the OTES-modified TESPA SAM and polymeric nanofilm. Cu-TESPA stands for copper surface covered with TESPA SAM, and Cu-TESPA-Heat represents copper surface covered with TESPA polymeric nanofilm.

modified surfaces are smaller than the values from OTS-modified surfaces, suggesting that the dielectric constants decline from the former surfaces to the latter. As a result, the long alkyl chain has great influence on the dielectric property of the bilayers.

The phase angle plot for the OTES modified TESPA SAM and the TESPA polymeric nanofilms without/with heating is displayed in Fig. 11. New time constants appear at the low frequency, however, are indistinct for all the surfaces. The new time constants of the OTS-modified surfaces can be observed easily (Fig. 5). The difference of the additional time constant between the OTS-modified interfaces and the OTES-modified ones, thereby suggests that the various interfacial phases form as a result of the reactions between OTS/OTES and SiOH groups from the TESPA-containing surfaces.

The new time constants and the original ones are mixed in TESPA-OTES system, indicating the property of the formed new phase resembles the ones from Cu-TESPA and Cu-TESPA-Heat. XPS and CA results in Part one have proved that SiOH groups and SiOSi plus SiOH groups exist on the above two surfaces. OTES belongs to a kind of alkoxy silanes, while OTS acts as one of chlorosilanes. Thus, the chemical difference determines the form of the new time constant.

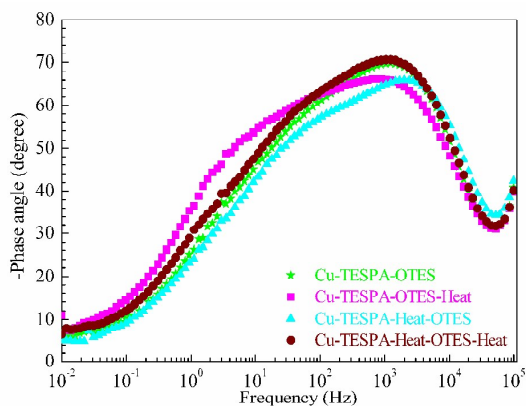


**Fig. 11** The phase angle plots of the TESPA SAM modified with OTES (Cu-TESPA-OTES), TESPA SAM modified with OTES plus heating (Cu-TESPA-OTES-Heat), the TESPA polymeric nanofilm modified with OTES (Cu-TESPA-Heat-OTES), and the TESPA polymeric nanofilm modified with OTES plus the following heating (Cu-TESPA-Heat-OTES-Heat) in 3.5 wt% NaCl solution. Cu-TESPA stands for copper surface covered with TESPA SAM, and Cu-TESPA-Heat represents copper surface covered with TESPA polymeric nanofilm.

### 3.2.3. Contact angles

The contact angle changes of the OTES-anchored surfaces were observed in Fig. 12. The slight enhancement of all OTES-containing surfaces indicates the successful assembly of OTES on the TESPA nanofilms with SiOH groups. The comparatively lower contact angles ( $< 90^\circ$ ) can be ascribed to the different surface free energy;

OTES with the short alkyl chain has a higher surface free energy than that of the OTS, bringing the lower contact angles.

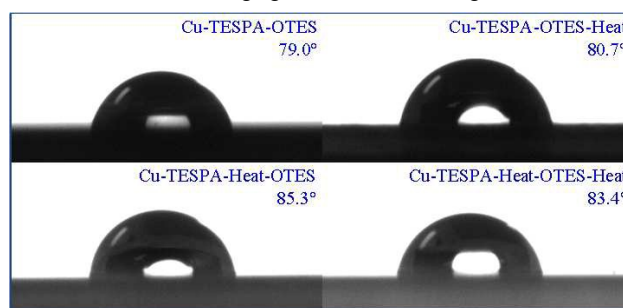


**Fig. 12** Contact angles of the OTES-modified TESPA SAM and the polymeric nanofilms. Cu-TESPA stands for copper surface covered with TESPA SAM, and Cu-TESPA-Heat represents copper surface covered with TESPA polymeric nanofilm.

### 3.2.4. Scanning electron microscopy (SEM) and energy dispersive X-ray spectroscopy (EDS)

Fig. 13 illustrates the SEM micrographs of 5  $\mu\text{m}$  and 1  $\mu\text{m}$  for the OTES-modified TESPA SAM and the TESPA polymeric nanofilm without/with heating. It is hard to find the white particles on all OTES-treated surfaces, indicative of the harmless of OTES as designed to anchor on the TESPA-containing surfaces. In comparison with the references (Fig. S6a to S6d), the bilayers of TESPA-OTES uniformly and densely cover copper surfaces. In the enlarged views, the fine streaks show up again on the surfaces of the OTES-modified TESPA SAM without heating (Fig. 13a'), and the OTES-modified TESPA polymeric nanofilm without/with heating (Fig. 13c' and 13d'). A new "interface phase" seems to shape with pores and cracks on OTES-modified TESPA SAM plus heating (Fig. 13b') and can be effortlessly differentiated from the others. Since this surface holds the most SiOH groups and was cured after the formation of the bilayer, the specific morphology and microstructure should be caused by these factors.

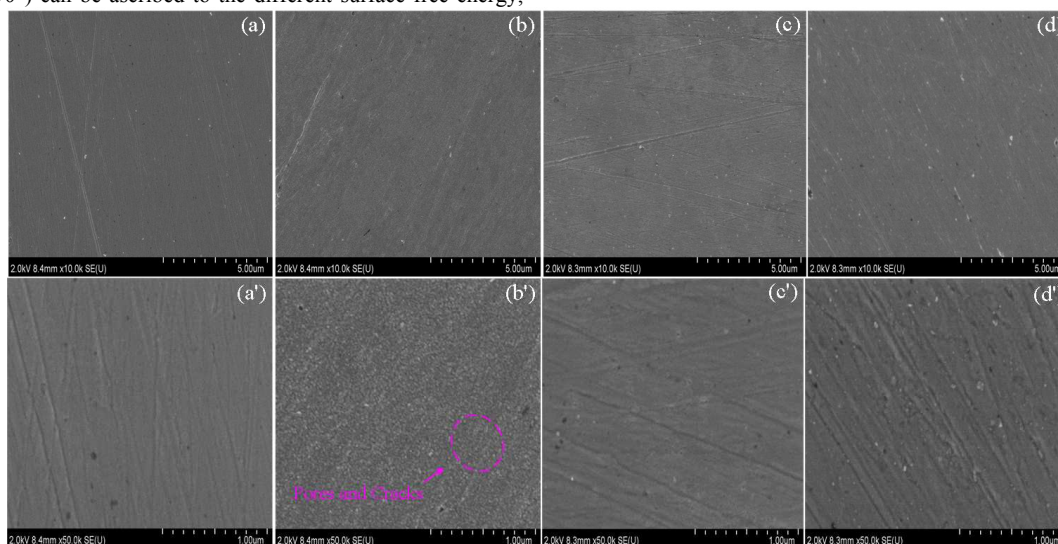


**Fig. 13** SEM micrographs of the (a) OTES-modified TESPA SAM

without heating, (b) OTES-modified TESPA SAM plus heating, (c) OTES-modified TESPA polymeric nanofilm without heating, and (d)

OTES-modified TESPAs polymeric nanofilm plus heating with 5  $\mu\text{m}$  and 1  $\mu\text{m}$ . Chinese Academy of Sciences.

We also carried out the energy dispersive spectroscopy of each OTES-modified surface in random areas for five times. Fig. S10a to Fig. S10d is just one representative of the each examination. The existing elements, their contents, and the coefficients ( $\sigma$ ) are also listed as the inset tables. The results for every surface are identical, indicating that the TESPAs-OTES are uniformly distributed on copper surface. Chlorine cannot be detected as expected. The reason why carbon contents from the OTS-treated surfaces outweigh that of the OTES-treated ones is that OTS possesses a longer alkyl chain.

### 3.3. The chemical mechanism and the prospects

By now, we can confirm that the TESPAs polymeric nanofilm not only resists corrosion but also serves as an activated interface on copper surface concurrently. Besides, the functionality of the TESPAs SAM is incidentally interpreted. Based on the above results, two models of Cu-TESPAs (the TESPAs self-assembled monolayer) and Cu-TESPAs-Heat (the TESPAs polymeric nanofilm) are proposed to be utilized in the following coating applications. If the reagents adopted to anchor onto the TESPAs-containing surfaces are detrimental to the substrate, Cu-TESPAs-Heat is preferable due to its protective ability; if the reagents are friendly, Cu-TESPAs act as a suitable interface full of SiOH activated sites. It should be emphasized that the molar concentration of TESPAs is small and only 3 mM in this investigation; the concentration was purposively chosen to highlight the protective and activating ability (other concentrations bring unobvious contrast effect). Therefore, it is easy to fabricate a multifunctional interface with excellent corrosion resistance and numerous silicon hydroxyl groups (activated sites), just by increasing it. Application experiment of this aspect will be covered in the future.

## 4. Conclusions

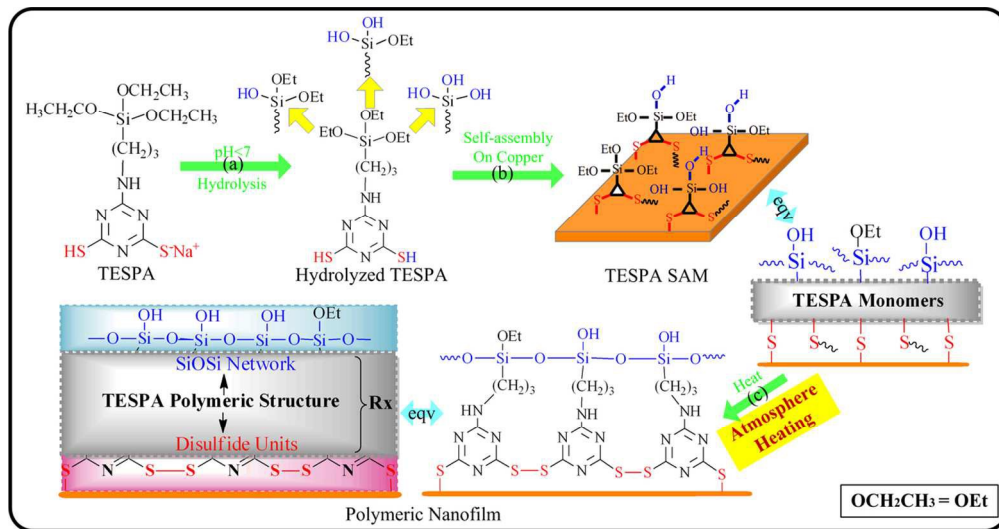
The multifunctionality of the TESPAs polymeric nanofilm has been confirmed by suitably selecting the modifiers to prepare the bilayers of TESPAs-OTS and TESPAs-OTES. The functionalized copper surface can resist corrosion and serve as an activated interface on copper surface simultaneously. Electrochemical tests and SEM show that the disulfide units (-SS-) and siloxane networks (SiOSi) from the polymeric nanofilm efficiently protect the surface in advance. The residual silanol groups (SiOH) serve as the activated sites for the subsequent chemical reactions. This functional interface could be utilized for further demanding industrial applications, such as colouring and paint processes that need a protective and activated medium for higher performances.

## Acknowledgements

The authors gratefully acknowledge financial supports provided by International S&T Cooperation Program of China (2013DFR40700), the National Natural Science Foundation of China (No. 21174034, No.51003019 and No. 51302280), the Natural Science Foundation of Qinghai (2014-ZJ-936Q), and Young Scholar Project of Qinghai Institute of salt lakes,

## Notes and references

1. Y. Wang, Z. Liu, D. Li, Y. Dong, W. Li and N. Li, *Corros. Sci.*, 2015, **98**, 382-390.
2. Y. Wang, Z. Liu, Y. Huang and Y. Qi, *Appl. Surf. Sci.*, 2015, **356**, 191-202.
3. J. Feng, G. Xu, Y. An, Y. and X. Zeng, *Colloid. Surface. A*, 2008, **316**, 194-201.
4. S. Pillai and R. K. Pai, *Ultramicroscopy*, 2009, **109**, 161-166.
5. M. Itoh, H. Nishihara and K. Aramaki, *J. Electrochem. Soc.*, 1995, **142**, 1839-1846.
6. R. Haneda and K. Aramaki, *J. Electrochem. Soc.*, 1998, **145**, 2786-2791.
7. M. Itoh, H. Nishihara and K. Aramaki, *J. Electrochem. Soc.*, 1995, **142**, 3696-3704.
8. S. Hsieh, W. J. Chao, P.-Y. Lin and C. W. Hsieh, *Corros. Sci.*, 2014, **80**, 427-433.
9. M. C. Brochier Salon and M. N. Belgacem, *Phosphorus. Sulfur.*, 2011, **186**, 240-254.
10. A. V. Benedeti, P. T. A. Sumodjo, K. Nobe, P. L. Cabot and W. G. Proud, *Electrochim. Acta.*, 1995, **40**, 2657-2668.
11. G. Kear, B. D. Barker and F. C. Walsh, *Corros. Sci.*, 2004, **46**, 109-135.
12. Y. Feng, W. K. Teo, K. S. Siow, K. L. Tan and A. K. Hsieh, *Corros. Sci.*, 1996, **38**, 369-385.
13. X. Wu, H. Ma, S. Chen, Z. Xu, A. Sui, X. Wu, S. Chen and A. Sui, *J. Electrochem. Soc.*, 1999, **146**, 1847-1853.
14. S. Li, Y. Wang, S. Chen, R. Yu, S. Lei, H. Ma and D. Liu, *Corros. Sci.*, 1999, **41**, 1769-1782.
15. M. D. G. Destrieri, Ouml, R. Vogelsang, L. Fedrizzi and F. Deflorian, *Prog. Org. Coat.*, 1999, **37**, 69-81.
16. E. Mccafferty and N. Hackerman, *J. Electrochem. Soc.*, 1972, **119**, 146-154.
17. B. N. Sahoo and B. Kandasubramanian, *RSC Adv.*, 2014, **4**, 22053-22093.



116x61mm (300 x 300 DPI)